Numerical Investigations of Detonation Reinitiation and Failure Modes from Mach Reflection

Shiyan Zhang[a], Shuyue Lai[b,*], Shizhi Tang[c], LinLin Yang[d], Fei Qi[b], Xiaohang Fang[c]

[a] *School of Aeronautics and Astronautics, Shanghai Jiao Tong University (SJTU), Shanghai, China*
[b] *School of Mechanical Engineering, Shanghai Jiao Tong University (SJTU), Shanghai, China*
[c] *Department of Mechanical & Manufacturing Engineering, University of Calgary, T2L 1Y6, Calgary, Canada*
[d] *Department of Engineering Science, University of Oxford, Oxford OX1 3PJ, UK*

Abstract

In this study, the stoichiometric hydrogen-air mixture detonation wave formations following a Mach reflection of two incident shocks are numerically studied. Compressible Navier-Stokes equations for two-dimensional reactive flow are solved via a high order numerical algorithm and the chemical reaction follows a newly calibrated chemical-diffusive model (CDM). By arranging the obstacle at the mid-height of the channel, detonation waves go through the process of propagation-overdriven-diffraction and the repeatable Mach reflection of the incident shocks can be captured at the trailing edge of the obstacle. From different geometric parameters of the obstacle, we observe different detonation propagation modes after Mach reflection: detonation reinitiation characterized by the transverse detonation waves, decaying shock decoupled with flame, and inert shock with no ignition corresponding well to the experimental findings. Relying on the high resolution of the numerical simulations, we are able to obtain critical information about the detonation wave formation processes, and the corresponding detailed mechanisms are analyzed for various modes. In order to quantitatively analyze the critical conditions for detonation reinitiation, we adopted a theoretical $D(\kappa)$ curve from the generalized ZND model based on the weakly-curved quasi-steady detonation by Kasimov and Stewart, which provides the relationship between critical detonation speed and curvature. Compared with different detonation modes in our simulations, the results show that $D(\kappa)$ curve from the ZND model gives a good indication of the detonation reinitiation region in the distribution map of velocity and curvature. The results indicate the current model can accurately determine the wave formation following a Mach reflection of two incident shocks. Furthermore, this presents the first numerical simulation supporting the previous experimental studies in confirming hydrogen detonations are in good agreement with the critical curvature predicted by the laminar ZND theory.

Keywords: Detonation wave; Mach reflection; Numerical simulation; Weakly-curved quasi-steady detonation;

* *Corressponding Author: laishuyue@sjtu.edu.cn*

Information for Colloquium Chairs and Cochairs, Editors, and Reviewers

1) Novelty and Significance Statement

For the first time in numerical simulation, a new obstacle configuration is added to the detonation channel to stably generate Mach reflection of incident shocks, and different modes of detonation reinitiation or failure are captured after the Mach reflection. Based on the asymptotic theory of self-sustained detonation, the critical $D(\kappa)$ curve for a weakly-curved detonation is used to predict various detonation propagation modes, which frames a critical region for detonation speed and shock front curvature. The study is significant in suggesting the predictive effectiveness of the $D(\kappa)$ curve theory for shock reflection in hydrogen mixtures can be used as the guidance for the design of hydrogen detonation and quenching industrial applications.

2) Author Contributions

- S. Zhang: Conceptualization, Investigation, Formal analysis, Data curation, Writing –original draft, Writing - Review & Editing.
- S. Lai: Conceptualization, Methodology, Investigation, Supervision, Writing –review & editing, Funding acquisition.
- S. Tang: Investigation, Data curation, Writing – review & editing.
- L. Yang: Investigation, Writing – review & editing.
- X. Fang: Conceptualization, Methodology, Supervision, Writing –original draft, Writing –review & editing, Funding acquisition.

3) A brief reason why the authors submit their work as an 8-page paper.

- The research is comprehensive and conducted with journal-quality rigor. An 8-page format provides the necessary space for a detailed explanation of the methodology, findings, and analysis, ensuring a thorough understanding of the topic.
- A detailed discussion of the critical $D(\kappa)$ curve theory, derived from the asymptotic analysis of self-sustained detonations, is essential. This theory has seen limited application in critical condition analysis, making its inclusion significant. The consistent results gathered from our study as well as previous supporting experiments suggest for hydrogen mixture such theory can be used as a valuable tool for the study of shock reflection.
- The paper emphasizes a numerical investigation of Mach reflection and detonation propagation modes in hydrogen mixtures, supported by experimental results for validation. This detailed approach warrants the extended format.

1. Introduction

Understanding the formation and propagation mechanisms of cellular detonation is vital for industrial safety concerning advanced energy systems and the design of a more efficient propulsion system. The cellular structure of a detonation wave refers to the formation of alternating high and low pressure zones behind the shock front, which is induced by the transverse wave interactions [1]. At each collision of the transverse waves, the Mach reflection influences the local thermodynamic conditions as well as the chemical kinetics. If a pair of opposite transverse detonations and the Mach stem coupled with flame form periodically, the cellular detonation structure can be maintained. However, if the chemical reaction behind the newly formed Mach stem is not intense enough to consume all the reactants, unburned gas will accumulate behind the shock front, and thus the detonation will attenuate to deflagration [2]. Therefore, identifying the factors that govern the distinction of the above two cases after Mach reflection is crucial for further understanding of the detonation propagation mechanism.

Various studies have focused on detonation quenching and reinitiation physics by considering shock reflection events under different configurations. When the cylindrical obstacle is used for experimental studies and numerical simulations [3, 4], reinitiation occurs as a result of detonation reflection from the obstacle or the channel boundary wall, where either a regular reflection or a Mach reflection is formed and leads to the reinitiation. For unstable detonations, reinitiation appears not only along the Mach stem, hot spots in the heated unburned reactants may also induce local explosions, where the regular and Mach reflections will alternate. Another category of experimental studies employs a concave configuration to explore the detonation reflection in an annular pipe [5–7]. Depending on the magnitude of the wedge angle, there is a shift from Mach reflection to regular reflection during detonation propagation. In this case, the traditional three-shock theory of planar detonation is no longer applicable. To date, relevant studies on the isolated effect of Mach reflections on detonation propagation are still scarce and necessitate further exploration.

Detonation reinitiation, as a significant phenomenon, has been suggested to have a complex mechanism and is influenced by multiple factors. Different obstacle configurations and channel confinements impact the strength and interactions of shock waves intensively [8, 9]. A set of critical length-scale criteria based on the detonation cell size (λ) has been developed. By adding inert porous filters or artificially setting the reactivity gradients to the channel, the role of the reactivity gradient on detonation re-initiation can be well explored [10, 11]. In addition, there is a variety of turbulent fluctuations as well as fluid instabilities that may also play a role in the promotion of detonation reinitiation [12]. With all these relevant affecting parameters, there lacks a unified theory predicting the onset, stability, and failure of detonation behaviors in various configurations. Derived from a one-dimensional detonation configuration, Kasimov and Stewart proposed a model to predict the detonation velocity (D) and the curvature (κ) of the detonation front using weakly-curved detonation front assumption and one-step chemical reaction model [13]. Recently, Farzane et al. [14] further verified this theory in their experimental study on the critical conditions for hydrogen detonation. Their study highlighted the critical curvature was well characterized by laminar ZND theory for weakly-curved detonation for the regular structure of hydrogen detonation. While the finding is significant, uncovering the detailed mechanisms of detonation wave formation near the shock reflection region can be challenging through experimental studies alone which motivated the current study.

In this study, we use high-fidelity numerical simulations to study the detonation attenuation and reinitiation processes in stoichiometric hydrogen-air mixtures following the Mach reflection of two incident shocks. A diamond shape obstacle, inspired by the experimental setup proposed by Farzane et al. [14], is placed in the channel to isolate detonation Mach reflection and to study its direct effects on detonation dynamics in a more controlled way. First, the use of the calibrated chemical diffusive model (CDM) [15] to capture the major detonation reinitiation or failure behaviors is validated. Then, the critical results of different detonation propagation modes observed by changing the geometric parameters are detailed. Furthermore, the asymptotic analysis method from Detonation Shock Dynamics (DSD) theory is developed and used to calculate the $D(\kappa)$ curve of the hydrogen mixture, which gives the critical envelop of shock speed and shock front curvature from generalized ZND model, examining the effectiveness of the $D(\kappa)$ theory for hydrogen detonation.

2. Numerical and Physical Models

2.1. Governing Equations

In this study, we solve the two-dimensional (2D) fully compressible Navier-Stokes equations, containing the conservations of mass, momentum, energy, and species, for the unsteady compressible reacting flow [16].

Stoichiometric premixed hydrogen-air mixture is used in this study, and the chemical reaction is described by the calibrated Chemical-Diffusive Model (CDM), which is precisely optimized with the additional detonation cell size by Lu et al. [15], so that the properties of the laminar flames (e.g. flame speed and thickness) and detonations (e.g. Chapman-Jouguet (CJ) speed, half-reaction thickness, and detonation cell size) calculated by CDM match the properties of the detailed chemical reaction simulations and the experimental results. Various prior studies have confirmed that the CDM model, in conjunction with these calibrated input parameters, can effectively capture the main features across a spectrum of problems, including laminar flame propagation, shock flame interactions, and detonations [17]. In this model, the chemical reaction rate follows the first-order Arrhenius equation:

$$\dot{\omega} = dY/dt = -A\rho Y \exp(-E_a/RT) \tag{1}$$

where A is the pre-exponential factor and E_a is the mixture activation energy. The diffusive characteristics in CDM are represented by the transport constants ν_0, D_0, and κ_0, which means kinematic viscosity, diffusion, and heat conductivity respectively, and are assumed to depend on temperature similarly:

$$\nu = \nu_0 \frac{T^{0.7}}{\rho}, \quad D = D_0 \frac{T^{0.7}}{\rho}, \quad \frac{K}{\rho C_p} = \kappa_0 \frac{T^{0.7}}{\rho} \tag{2}$$

where $C_p = \gamma R/M(\gamma - 1)$ is the specific heat at a given pressure and the temperature dependence of these coefficients is chosen to 0.7 exponential term in this reactive system[18]. The interrelationship among ν_0, D_0, and κ_0 is

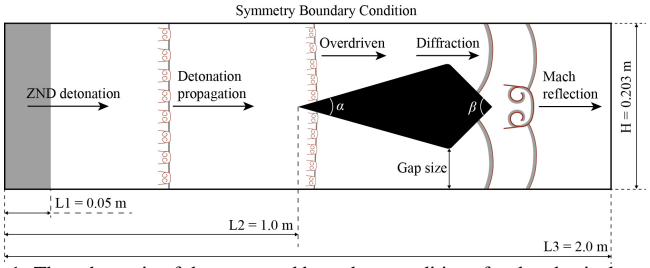

Fig. 1: The schematic of the setup and boundary conditions for the physical model.

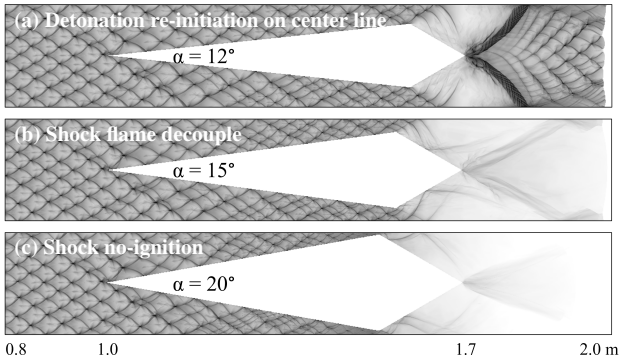

Fig. 2: Global numerical soot foils for different detonation modes. The figure size is 1.2 m $\times$ 0.203 m.

elucidated through three dimensionless parameters $Lewis$, $Prandtl$, and $Schmidt$ numbers:

$$\mathrm{Le} = \frac{K}{\rho C_p D} = \frac{\kappa_0}{D_0}, \quad \mathrm{Pr} = \frac{\rho C_p \nu}{K} = \frac{\nu_0}{\kappa_0}, \quad \mathrm{Sc} = \frac{\nu}{D} = \frac{\nu_0}{D_0} \tag{3}$$

In order to solve the above governing equations, a fifth-order WENO numerical algorithm with HLLC fluxes is used for the spatial discretization, and a third-order Runge-Kutta algorithm is used for time advancement. The calculations are performed using a uniform grid with a resolution of 100 μm, which corresponds to about 3-4 grid points per laminar flame thickness and about 10-20 cells per half-reaction thickness. Previous studies have shown that the given grid size can capture the main characteristics of flame acceleration, DDT initiation, and detonation propagation for stoichiometric hydrogen-air mixtures [19]. For dealing with obstacles in the flow field, the Immersed Boundary Method (IBM) is used to differentiate between solid-phase obstacles and gas-phase reactive flows.

2.2. Computational Setup

In this study, detonation propagates in an obstructed channel filled with stoichiometric hydrogen-air mixture. The computational model is shown in Fig.1, with the channel height of $H = 0.203$ m, the total length of $L3 = 2.0$ m, and a obstacle locating in the region of $x = 1.0$ m to $x = 1.7$ m on the channel center line. Experiments have shown that this setup yields sustainable Mach reflection after the obstacle [14]. The obstacle isolates two converging-diverging semi-channels, where the detonation waves undergo the overdriven-diffraction process and interact at the trailing edge of the obstacle, and produce the targeting Mach reflection.

Detonation initiation is achieved by the Zeldovich-von Neumann-Döring (ZND) solution with perturbation applied at $x = 0.05$ m on the left side of the channel and then propagates to the right side. The diamond shape object is placed 1 m away from the left boundary, which is far enough for the detonation to stabilize before it interacts with the obstacle. Symmetric conditions are used at all boundaries, and the surface of the obstacle is treated as a no-slip adiabatic wall. The obstacle β angle at the trailing edge is fixed at 60°, which is chosen to get the backward-propagating Mach stem as far as possible after the incident waves collide with each other [20]. By adjusting the α angle at the leading edge, different detonation re-initiation or failure modes are obtained. The experimental parameters and the main phenomena are listed in Table 1.

3. Results and Discussion

In this section, we first present the detonation modes observed in different obstacle configurations. Figure 2 shows the global smoke foils corresponding to three detonation modes, with the x axis ranging from 0.8 to 2.0 m. The detonation forms a relatively stable cellular structure before it reaches the obstacle. Starting from $x = 1.0$ m, the detonation wave is separated into two isolated channels and continuously compressed to an overdriven state. After that, the detonation waves begin to diffract as the channels expand, accompanied by the detonation attenuation and shock flame decoupling to a certain degree. At the trailing edge of the obstacle ($x = 1.7$ m), the incident shocks collide and reflect, leading to different detonation modes downstream. For case (i), as a representative of the reinitiation mode, detonation reinitiation first appears on the centerline of the channel,

Table 1: Geometric parameters for simulation and the corresponding detonation propagation mode.

Case	α [deg]	Gap size [m]	Mode
(i)	10	0.0483	Detonation reinitiation
(ii)	12	0.0393	Detonation reinitiation
(iii)	15	0.0265	Shock flame decouple
(iv)	20	0.0069	Shock no ignition

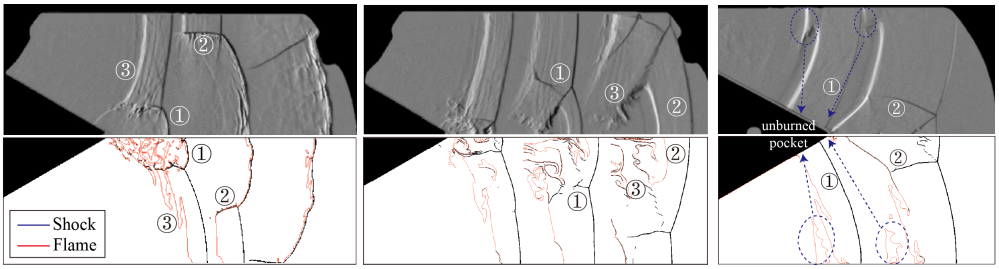

(a) $\alpha = 10°$, detonation reinitiation (b) $\alpha = 15°$, shock flame decouple (c) $\alpha = 20°$, no ignition

Fig. 3: Comparisons of experimental results (upper) [14] and simulation modes (lower). Shocks are represented by iso-surfaces of numerical schlieren, and the flame surface is defined as Y = 0.5.

and then gradually develops to the whole channel. Starting from the expansion region of the obstacle, the fully quenching area can be observed in Fig.2 (a), following the transverse detonations with secondary cellular structures. After the transverse detonations, the reflective Mach shock passes through no-cell region, growing-cell region [11], and finally reestablishes a detonation wave with stable cellular structures. However, the reflections from boundary wall will provide further energy for the propagation of detonation and thus influence the cellular structure. When the angle increases to $\alpha = 15°$, the shock front decouples with the flame, and the detonation wave quenches. Further increasing α to 20°, detonation propagates in the form of inert shock without ignition behind the obstacle. The mechanism of each detonation mode will be detailed in later sections.

Figure 3 shows the comparisons of local characteristics during Mach reflection between our simulated results and previous experiments [14]. Note that the fuel mixtures used in the current simulation and in the experiment are different ($2H_2/O_2/2Ar$ in the experiment). The key features observed in the three detonation modes are, however, consistent with each other. For the reinitiation mode, the curved Mach stem (marked ①) gradually evolves, accomplished by the transverse detonation waves (②) along the induction zone between the shock front and flame surface (③). In Fig.3 (b), flame decouples with the shock front (①) before Mach reflection, and unburned gas accumulates behind the curved Mach stem (②) with the slip line (③) separating the location of flame. For the no-ignition mode in Fig.3 (c), flame lags considerably behind the shock front (①), and leaves the unburned pockets near the boundary wall. After the reflection, the inert Mach stem propagates with the inert transverse shock (②).

3.1. Detonation Reinitiation Mode

Figure 4 shows the temperature fields of detonation reinitiation mode at different instants. It can be seen that in the obstacle expansion region, the flame front decouples from the shock front and forms a series of reaction tongues, indicating the occurrence of detonation attenuation. The first collision of the incident shocks (IS) can be observed at $t = 0.847$ ms, which gives rise to significant increase in local pressure and temperature and then generates the ignition kernel marked F1 in Fig. 4 (b2). A second collision of the extended incident shocks, which are separated by the reaction tongues, forms the new ignition kernel marked F2 in the next frame. In Fig. 4 (c-d), the inner ignition kernel F1 induces the local explosion event and consumes the pocket of unburned gas, while the outer ignition kernel F2 forms the triple points of Mach reflection. At $t = 0.861$ ms, the formation of the curved Mach stem can be observed. The transverse wave is divided into two parts at this time: the reactive part connecting with the inner localized explosion, and the inert part from outer Mach reflection. As the Mach stem propagates to the right, the standard transverse detonations are formed at $t = 0.864$ ms, which contains the extended transverse detonation part additionally. This extended wave is an oblique shock wave and reacting slip line that connects the triple point to the transverse detonation wave [21]. This feature can be difficult to observe through experimental studies due to the challenging conditions of the experiments. In Fig.4 (f), two apparent transverse detonation waves (TD) move along the induction zone. They are followed by transverse shocks in the flame. The transverse detonations consume almost all the reactants in the induction zone, leaving a non-reactive tail in the vicinity of the triple point. These typical features of this Mach structure are similar to the numerical results from Gamezo et al. [22] and experimental phenomena from Xiao et al. [23]. The generation of this non-reactive tail is a result of the relatively low temperature region between the leading shock and the transverse detonation from double Mach reflection. The structure of the vortex system induced by the Kelvin-Helmholtz instabilities can be observed in the shear layer between the Mach

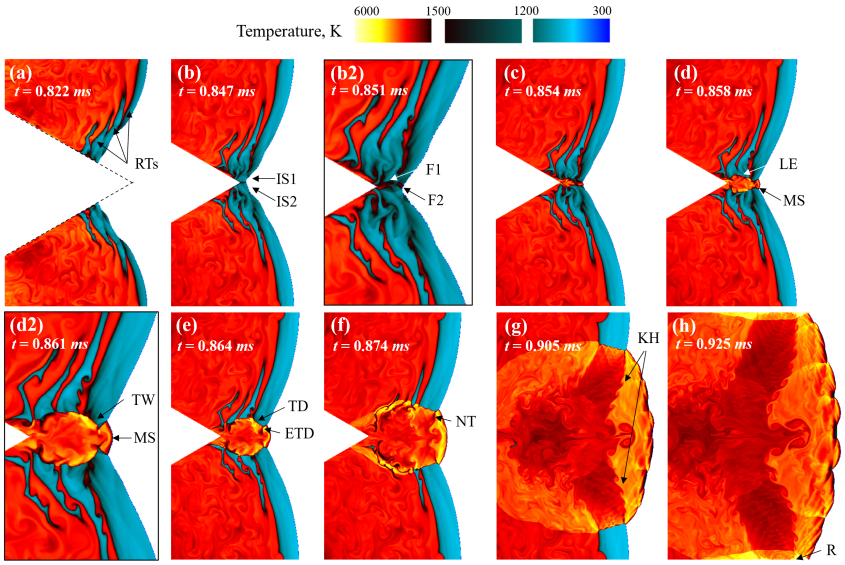

Fig. 4: Temperature fields of detonation reinitiation mode of different time steps. The y axis is the full span of the setup channel, except for (b2) and (d2) figures in black frame that are zoomed in for more details. (RTs: reaction tongues, IS: shock wave, F: ignition kernel, LE: local explosion, MS: Mach stem, TW: transverse wave, TD: transverse detonation, ETD: extended transverse detonation, KH: Kelvin-Helmholtz instability, NT: non-reactive tail, R: reflection.)

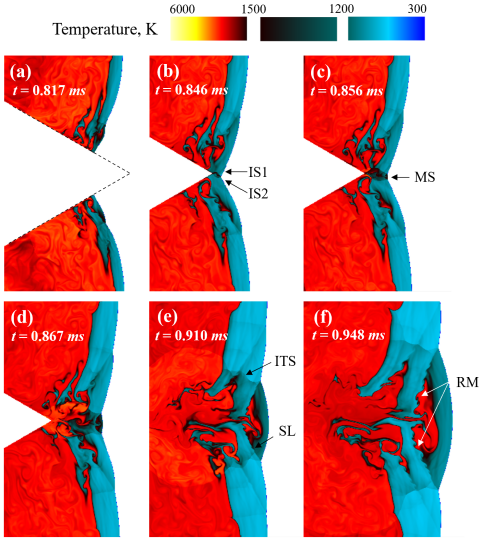

Fig. 5: Temperature fields of shock flame decouple mode at different time steps. (IS: shock wave, MS: Mach stem, SL: slip line, ITS: inert transverse shock, RM: Richtmyer–Meshkov instability)

shock region and the transverse waves. As the transverse detonation waves propagate, secondary reflections occur after their collisions with the channel wall. It is also worth noting that compared to hydrocarbon experiments where the reaction front is characterized by significant hydrodynamics fluctuations and unreacted pockets, the reaction fronts seen in our numerical simulations are rather inline with laminar reaction front characteristics. Such differences between hydrogen and other hydrocarbon in detonation wave formation are also highlighted in previous [14].

3.2. Detonation Failure Mode

The shock-flame decoupling mode for case (iii), $\alpha = 15°$, is shown in Fig.5, where the detonation wave decays to the shock followed by the reaction zone behind it after the Mach reflection. Under this condition, the detonation wave first shows more significant attenuation in the expansion region of the obstacle. At $t = 0.846$ ms, the incident shocks collide at the trailing edge of the obstacle, where the Mach reflection occurs. The Mach stem continuously evolves to the leading shock front with a certain curvature. The flame surface always lags behind the leading shock, demonstrating the decoupling of shock and flame. In Fig.5 (e), it can be seen that the inert transverse shocks propagate along the induction zone behind the slip line. The heated gas accumulates in the form of jet flow behind the Mach shock over time in the presence of Richtmyer–Meshkov instabilities. Although this instability promotes the interaction of the turbulent flame with the Mach shock induced zone, the detonation in this case decays to a failure mode with no reinitiation. This differs from previous experiments involving hydrocarbon-oxygen detonations, such as stoichiometric mixtures of CH_4, C_2H_4, C_2H_6, and C_3H_8. These mixtures have been observed to re-amplify after traveling significant distances beyond obstacles, with the turbulent reaction zone structure remaining closely coupled to the leading shock. For hydrocarbons, it is suggested that the formation of strong jets behind periodically formed Mach shocks provides localized enhancement of reactivity through turbulent mixing [24].

By increasing α to 20°, the detonation propagation mode changes to an inert shock without ignition behind the Mach reflection, as shown in Fig.6. The decoupling of the shock front and flame is more pronounced in the expansion region

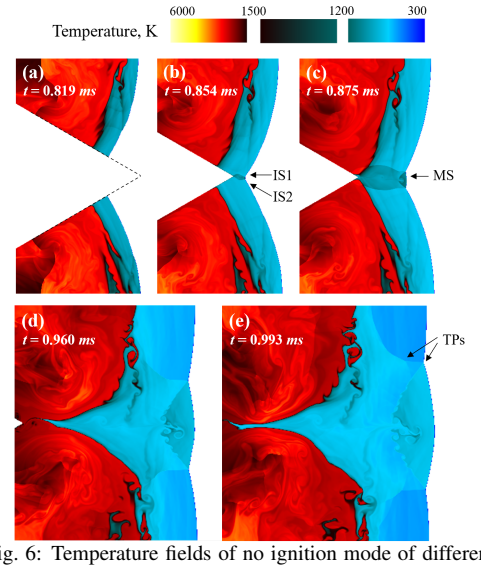

Fig. 6: Temperature fields of no ignition mode of different time steps. (IS: shock wave, MS: Mach stem, TPs: triple points.)

of the obstacle. At the trailing edge of the obstacle, two incident shocks interact with each other, forming an inert Mach wave. Due to the long decoupling distance between the shock and the flame, there is no re-ignition event behind the Mach shock in the propagation process. At $t = 0.993$ ms, the double triple points configuration becomes apparent in Fig.6 (e), and eventually merges as the shock wave propagates downstream.

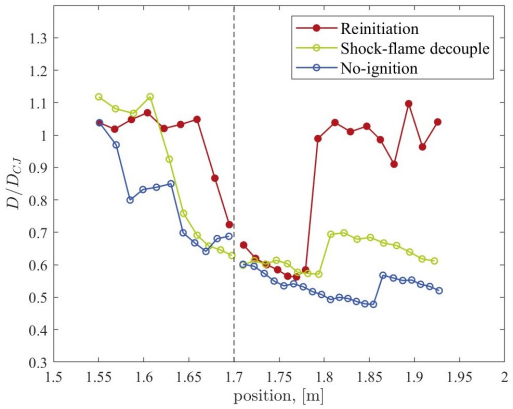

Fig. 7: Detonation velocity evolution along x axis positions, dashed line represents the trailing edge of the obstacle (1.7 m).

Figure 7 shows the detonation velocity evolution from decaying process to the Mach shock reestablishment. The velocities of the incident shock in the expansion region of the obstacle are measured along the channel top wall and the velocities of the Mach shock are measured along the center line. A significant deceleration of the local velocity profile along the expansion region occurs, with the velocity decreasing to 0.6-0.7D_{CJ} for all the cases. After the interaction of the two decaying shocks, the compression effect and reinitiation process take a period of time and form a new Mach shock. For the detonation reinitiation case, the shock speed rapidly increases to nearly CJ speed and then oscillates near the CJ speed. For the shock-flame decouple mode, the detonation velocity increases to about 0.7D_{CJ} after Mach reflection and then decelerates as the unburned gas accumulates behind the shock front. For the no-ignition mode, the shock velocity remains below 0.6D_{CJ} after reflection and continues to decay as the formation of inert shock.

3.3. Critical Conditions with $D(\kappa)$ Curve

In this section, we first give a brief introduction to the asymptotic theory of self-sustained detonation in the Detonation Shock Dynamics (DSD) theoretical framework [13, 25, 26], which defines a virtual sonic locus in the detonation waves. This locus physically is where the Mach number in shock-attached frame equals to sonic speed, and mathematically it is a characteristic surface which serves as the information boundary for the reaction zone initiated by the leading shock. For a self-sustaining detonation, the shock speed must always exceed the local sonic speed behind the shock. The sonic locus is crucial for determining whether the detonation wave can propagate stably. If the shock front decelerates and reaches a speed below the sonic speed, the detonation will fail and combustion will revert to subsonic deflagration.

The analysis reveals the intrinsic relationship in shock speed, shock acceleration, and the shock front curvature ($\dot{D} = a_1\dot{\omega} - a_2\kappa$, $\dot{\omega}$ is reaction rate and κ is shock front curvature). Heat release from chemical reaction gives positive effects to the shock acceleration, while the dissipation from curved expansion gives negative effects. Two competing mechanisms finally reach a balanced state during the detonation propagation.

For the quasi-steady (acceleration $\dot{D}$ equals to 0) one-dimensional reacting flow behind the curved shock front of the detonation wave, the governing equations in the shock-attached frame can be expressed as a set of ordinary differential equations (ODEs) [23]:

$$\frac{dp}{dt} = -\rho u^2 \frac{\dot{\sigma}_{re} - \dot{\sigma}_A}{1 - M^2} \tag{4}$$

$$\frac{d\rho}{dt} = -\rho \frac{\dot{\sigma}_{re} - M^2\dot{\sigma}_A}{1 - M^2} \tag{5}$$

$$\frac{du}{dt} = u \frac{\dot{\sigma}_{re} - \dot{\sigma}_A}{1 - M^2} \tag{6}$$

$$\frac{dy}{dt} = \frac{W_i \dot{w}_i}{\rho}, \quad (i = 1, ..., N_s) \tag{7}$$

$$\dot{\sigma}_{re} = \sum_{i=1}^{N_s} \left(\frac{W}{W_i} - \frac{h_i}{C_p T}\right) \frac{dy_i}{dt},$$

$$\dot{\sigma}_A = K(D_s - u) \tag{8}$$

where ρ, p, M, C_p, h_i, y_i, W_i, $\dot{w}_i$, and N_s are the mixture density, pressure, local Mach number ($M = u/c$), specific heat at constant pressure, enthalpy of species i, species mass fraction, molecular weight of species i, molar production rate of species i, and the total number of species. u is the velocity in shock-attached frame, which means $u = v - D_s$ where v is the normal velocity in lab frame and D_s is the detonation shock velocity. $\dot{\sigma}_{re}$ is the thermicity, $\dot{\sigma}_A$ is the

rate of lateral strain, and κ is the curvature of the detonation front. The thermicity represents heat release from chemical reaction which accelerates the gas to transonic and supersonic state, while the lateral strain from diffraction plays a role of deceleration. The ODEs system's singular point at $M = 1$ ($u = c$) means the gas reaches sonic locus, and at this locus $\dot{\sigma}_{re}$ and $\dot{\sigma}_A$ reach a balance state, which names generalized CJ condition.

In order to get the relationship between detonation speed and the shock front curvature from the generalized ZND model, we solve the above equations on the framework of *Cantera*, and use the *Shock and Detonation Toolbox* (SD Toolbox) to calculate the jump condition at two sides of the shock. A detailed reaction mechanism *San Diego* [27] is adapted for the simulation of hydrogen-air mixture combustion at 1 atm. For a given detonation speed (D_s, focusing on 0.8-0.99 D_{CJ} in our calculation), traverse a certain array of curvature outside the time iteration loop of the ODEs to find the critical curvature corresponding to the current detonation speed. If the curvature is larger than critical value, the gas speed behind the shock cannot accelerate to the sonic locus ($M = 1$). In contrast, if the curvature is smaller, the heat release from chemical reaction overcomes the negative effects of wave expansion and the system is not balanced at singular point.

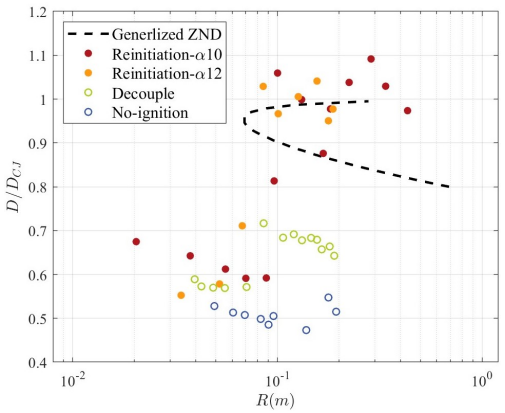

Fig. 8: The nondimensional detonation speed versus shock front curvature and predictions derived from the Generalized ZND model.

Compared with the ZND solution, the results from our simulations are shown in Fig.8, which contains two cases of detonation reinitiation in solid circle and two cases of detonation quenching in hollow circle. The x axis is the curvature radius ($R = 1/\kappa$) and the y axis is the nondimensional velocity measured on the centerline of the channel after Mach reflection. The shock front curvature is obtained by means of image processing and fitting from SciPy. For the two detonation reinitiation cases, corresponding to case (i) and (ii) in Fig.2, when the point touches the dashed curve, thermicity balances the effect of curvature, indicating a successful reinitiation of detonation with its velocity oscillating near the CJ speed. But for two failure modes, the velocity decreases in an oscillatory manner as the curvature radius amplifies, and it will never reach the lower branch of ZND curve which means detonation attenuates to shock-flame decoupling state or even inert Mach shock with no ignition, and reinitiation will not occur under these circumstances. For the decoupling case, despite the fact that we find some promotion mechanisms in the temperature fields, the detonation cannot be reinitiated and sustained. This is because the heat release due to chemical reaction, which represents the primary factor for acceleration, cannot balance the negative effects of diffusion. Moreover, the absolute nondimensional velocity of no-ignition mode is smaller than that of shock-flame decoupling, which means the detonation attenuation is more significant in this case.

From these results, it is concluded that the transition between detonation formation and ignition shows a stronger correlation with the critical curvature. This agrees well with the curvature concept proposed by Kasimov and Stewart for quasi-steady curved detonations. Numerical results for hydrogen-air mixtures using CDM aligned remarkably well with the critical curvature predicted by ZND theory. It is worth noting here that Xiao et al. previously experimentally examined the similar diffusive phenomena of gaseous detonations in the channel with exponentially enlarging cross-sections, which confined the detonation lateral strain and so that the velocity curvature follows better with the theoretical D(κ) curve compared with our numerical results [23]. For the cases in this study, the Mach shock is not constrained by the channel from emergence to the detonation reinitiation, and thus the velocity may oscillate around the theoretical curve which is consistent with previous experimental results [14]. Nevertheless, it is significant in our study confirming that the critical curvature for weakly-curved detonations in the regular structure hydrogen–air mixture can be well predicted by the laminar ZND theory. Thus the use of such criteria can serve as a starting point for the design of numerical simulations.

4. Summary and Conclusions

The detonation attenuation and reinitiation process in an obstructed channel filled with stoichiometric hydrogen-air mixture is study using a high-fidelity two-dimensional simulation with a calibrated chemical diffusive model (CDM). The channel is divided into two converging-diverging semi-channels by placing a diamond shape obstacle, creating a controllable Mach reflection process. Three different propagation modes behind the obstacle are captured in the current simulations: detonation reinitiation mode, shock flame decoupling mode, and no ignition mode. The global and local characteristics of different detonation modes are validated by comparing with an earlier experiment. At the same time, we captured the detailed process of detonation Mach reflection, highlighting the important role of transverse detonation waves in the reinitiation process after Mach reflection of the two incident shocks. Moreover, compared to hydrocarbon experiments, where the reaction front is characterized by significant hydrodynamic fluctuations and unreacted pockets, the reaction fronts observed in our numerical simulations for hydrogen-air mixtures align more closely with laminar reaction front characteristics consistent with previous experiments.

Based on the theory of one-dimensional quasi-steady detonation, the $D(\kappa)$ curve using generalized ZND model for hydrogen-air mixture detonation under atmospheric conditions is calculated, which envelops the critical region in the figures of detonation speed and shock front curvature. Two competing mechanisms, chemical reaction heat release and expansion effect of curved shock front, reach a dy-

namic equilibrium state between the detonation reinitiation and failure modes. Comparing with our simulation results, the theoretical curve based on one-dimensional quasi-steady detonation matches well, which further validates the effectiveness of the quasi 1D $D(\kappa)$ theory in predicting a multi-dimensional hydrogen detonation behavior.

Declaration of Competing Interest

The authors declare that they have no known competing financial interests or personal relationships that could have appeared to influence the work reported in this paper.

Acknowledgments

This study was supported by the National Science Foundation of China (Grant No. 12002207), the Natural Sciences and Engineering Research Council of Canada (Grant No. RGPIN-2023-03309) and Alberta Innovates. This work is also partially supported by SJTU Kunpeng&Ascend Center of Excellence, and SJTU supercomputing resources (https://hpc.sjtu.edu.cn/). We also would like to acknowledge Dr. Farzane Zangene from University of Ottawa for the discussion on DSD theoratical framework development.

References

[1] B. M. Maxwell, R. R. Bhattacharjee, S. S. M. Lau-Chapdelaine, S. A. E. G. Falle, G. J. Sharpe, M. I. Radulescu, Influence of turbulent fluctuations on detonation propagation, Journal of Fluid Mechanics 818 (2017) 646–696.

[2] M. I. Radulescu, G. J. Sharpe, C. K. Law, J. H. S. Lee, The hydrodynamic structure of unstable cellular detonations, Journal of Fluid Mechanics 580 (2007) 31–81.

[3] R. Bhattacharjee, S. Lau-Chapdelaine, G. Maines, L. Maley, M. Radulescu, Detonation re-initiation mechanism following the Mach reflection of a quenched detonation, Proc. Combust. Inst. 34 (2) (2013) 1893–1901.

[4] S. Tang, S. Zhang, S. Lai, X. Fang, Effect of activation energy on detonation cellular dynamics and re-initiation behaviors, AIAA Journal 0 (0) (2025).

[5] Y. Fortin, J. Liu, J. H. Lee, Mach reflection of cellular detonations, Combust. Flame 162 (3) (2015) 819–824.

[6] J. Li, H. Ren, X. Wang, J. Ning, Length scale effect on Mach reflection of cellular detonations, Combust. Flame 189 (2018) 378–392.

[7] Z. Yang, B. Zhang, H. D. Ng, Experimental observations of gaseous cellular detonation reflection, Proc. Combust. Inst. 40 (1) (2024) 105519.

[8] D. Jun, D. Kwon, B. J. Lee, Numerical study on the reinitiation mechanism of detonation propagating through double slits in a planar channel, Combust. Flame 261 (2024) 113271.

[9] G. Rainsford, D. J. S. Aulakh, G. Ciccarelli, Visualization of detonation propagation in a round tube equipped with repeating orifice plates, Combust. Flame 198 (2018) 205–221.

[10] D. Tropin, K. Vyshegorodcev, Numerical simulation of interaction of cellular detonation wave with systems of inert porous filters, International Journal of Hydrogen Energy 48 (48) (2023) 18454–18485.

[11] X. Jia, Y. Xu, H. Zheng, H. Zhang, Direct detonation initiation in hydrogen/air mixture: effects of compositional gradient and hotspot condition, Journal of Fluid Mechanics 970 (2023) A22.

[12] S. S.-M. Lau-Chapdelaine, M. I. Radulescu, Viscous solution of the triple-shock reflection problem, Shock Waves 26 (5) (2016) 551–560.

[13] A. R. Kasimov, D. S. Stewart, Asymptotic theory of evolution and failure of self-sustained detonations, Journal of Fluid Mechanics 525 (2005) 161–192.

[14] F. Zangene, M. I. Radulescu, The critical conditions for the re-ignition and detonation formation from Mach reflections of curved decaying shocks, Proc. Combust. Inst. 40 (1-4) (2024) 105774.

[15] X. Lu, C. R. Kaplan, E. S. Oran, Calibrating the chemical-diffusive model using the detonation cell data, in: AIAA Scitech 2021 Forum, American Institute of Aeronautics and Astronautics, 2021.

[16] S. Lai, S. Tang, C. Xu, N. Sekularac, X. Fang, Computational diagnostics for flame acceleration and transition to detonation in a hydrogen/air mixture, Combust. Flame 258 (2023) 113054.

[17] H. Xiao, E. S. Oran, Shock focusing and detonation initiation at a flame front, Combust. Flame 203 (2019) 397–406.

[18] D. Kessler, V. Gamezo, E. Oran, Simulations of flame acceleration and deflagration-to-detonation transitions in methane–air systems, Combust. Flame 157 (11) (2010) 2063–2077.

[19] X. Lu, C. R. Kaplan, E. S. Oran, A chemical-diffusive model for simulating detonative combustion with constrained detonation cell sizes, Combust. Flame 230 (2021) 111417.

[20] J. M. Austin, The role of instability in gaseous detonation, Ph.D. thesis, California Institute of Technology (2003).

[21] G. Floring, M. Peswani, B. Maxwell, On the role of transverse detonation waves in the re-establishment of attenuated detonations in methane–oxygen, Combust. Flame 247 (2023) 112497.

[22] V. Gamezo, A. Vasil'ev, A. Khokhlov, E. Oran, Fine cellular structures produced by marginal detonations, Proc. Combust. Inst. 28 (1) (2000) 611–617.

[23] Q. Xiao, M. I. Radulescu, Dynamics of hydrogen–oxygen–argon cellular detonations with a constant mean lateral strain rate, Combust. Flame 215 (2020) 437–457.

[24] M. Saif, W. Wang, A. Pekalski, M. Levin, M. I. Radulescu, Chapman–jouguet deflagrations and their transition to detonation, Proc. Combust. Inst. 36 (2) (2017) 2771–2779.

[25] M. I. Radulescu, B. Borzou, Dynamics of detonations with a constant mean flow divergence, Journal of Fluid Mechanics 845 (2018) 346–377.

[26] S. I. Jackson, C. Chiquete, M. Short, An intrinsic velocity–curvature–acceleration relationship for weakly unstable gaseous detonations, Proc. Combust. Inst. 37 (3) (2019) 3601–3607.

[27] F. Williams, Chemical-kinetic mechanisms for combustion applications. san diego mechanism web page, mechanical and aerospace engineering (combustion research), university of california at san diego.
URL (http://combustion.ucsd.edu).